

Article

Insight into Rare Structurally Characterized Homotrimeric Cu^{II} Non-Symmetric Salamo-Based Complex

Yun-Dong Peng, Ruo-Yu Li, Peng Li and Yin-Xia Sun *

School of Chemical and Biological Engineering, Lanzhou Jiaotong University, Lanzhou 730070, China; pengyundong6@126.com (Y.-D.P.); 0219577@stu.lzjtu.edu.cn (R.-Y.L.); 0219532@stu.lzjtu.edu.cn (P.L.)

* Correspondence: sunyinxia@mail.lzjtu.cn; Tel.: +86-931-4938755

Abstract: A rare homotrimeric Cu^{II} salamo-based complex [Cu₃(L)₂(μ-OAc)₂(H₂O)₂]·2CHCl₃·5H₂O was prepared through the reaction of a non-symmetric salamo-based ligand H₂L and Cu(OAc)₂·H₂O, and validated by elemental analyses, UV-Visible absorption, fluorescence and infrared spectra, molecular simulation and single-crystal X-ray analysis techniques. It is shown that three Cu^{II} atoms and two wholly deprotonated ligand (L)²⁻ moieties form together a trinuclear 3:2 (M:L) complex with two coordination water molecules and two bi-dentate bridging μ-acetate groups (μ-OAc⁻). Besides, the Hirshfeld surface analysis of the Cu^{II} complex was investigated. Compared with other ligands, the fluorescent strength of the Cu^{II} complex was evidently lowered, showing that the Cu^{II} ions possess fluorescent quenching effect.

Keywords: non-symmetric salamo-based ligand; Cu^{II} complex; crystal structure; fluorescence property; the Dmol³ module



Citation: Peng, Y.-D.; Li, R.-Y.; Li, P.; Sun, Y.-X. Insight into Rare Structurally Characterized Homotrimeric Cu^{II} Non-Symmetric Salamo-Based Complex. *Crystals* **2021**, *11*, 113. <https://doi.org/10.3390/cryst11020113>

Received: 17 January 2021

Accepted: 22 January 2021

Published: 26 January 2021

Publisher's Note: MDPI stays neutral with regard to jurisdictional claims in published maps and institutional affiliations.



Copyright: © 2021 by the authors. Licensee MDPI, Basel, Switzerland. This article is an open access article distributed under the terms and conditions of the Creative Commons Attribution (CC BY) license (<https://creativecommons.org/licenses/by/4.0/>).

1. Introduction

Both the salen-based ligands and their derivatives have shown strong development potential in the research of materials chemistry, coordination chemistry, and environmental monitoring for decades because of their good application prospects in organic catalytic synthesis, molecular magnetic properties, and luminescent properties [1–5], which, owing to their N₂O₂-donor structure, usually have excellent coordination ability to transition metal ions for various structural novel complexes (derivatives) [6–11].

The salamo-based ligands with strong stability and multifunctional chelating ability have also been studied as a significant class of organic compounds containing N₂O₂-donor groups [12–18]. When compared with salen-based ligands, the salamo-based compounds and their complexes have been applied to ion recognition [19,20], optics [21], electrochemistry [22], magnetism [23,24], biochemistry [25,26], catalysis [27,28], supermolecular construction [29,30], and other fields [31–38], which are expected to give the salamo-based ligands and their derivatives good development potential to become one of the new research hotspots of coordination chemistry.

The fluorescence on-off phenomenon in the coordination reaction of the salamo-based ligands and Cu^{II} ions can be used to identify and detect Cu^{II} ions in the environment [39–42]. According to a large amount of preliminary research works [43–49], here, a non-symmetrical salamo-derived compound H₂L was prepared, several single crystals of its Cu^{II} complex were obtained by natural evaporation method in chloroform/ethanol mixed solvent at room temperature in about one month, and the structures and properties of H₂L and its Cu^{II} complex were further characterized by various modern analytical techniques.

2. Experimental Section

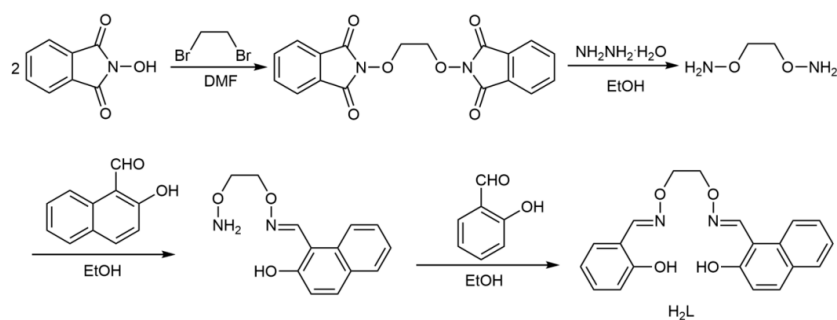
2.1. Materials and Instruments

All chemical solvents and raw materials were acquired from mercantile sources and could be used directly. Elemental analysis of Cu^{II} was tested via IRISER/S-WP-1 ICP atomic

emission spectrometer (Elementar, Berlin, Germany), and associated elemental analyses for carbon, hydrogen, and nitrogen were carried out by GmbH VariuoEL V3.00 automatic elemental analysis instrument (Elementar, Berlin, Germany). The study of IR spectra were recorded according to a Bruker VERTEX70 FT-IR spectrophotometer, with samples prepared as CsI (100–500 cm^{-1}) and KBr (400–4000 cm^{-1}) pellets (Bruker AVANCE, Billerica, MA, USA). The UV-Visible spectra were acquired from a Shimadzu UV-3900 spectrometer (Shimadzu, Tokyo, Japan). The ^1H NMR spectra were tested via German Bruker AVANCE DRX-400/600 spectrometer (Bruker AVANCE, Billerica, MA, USA). Fluorescent spectra of H_2L and its Cu^{II} complex were conducted from an F-7000FL spectrophotometer (Hitachi, Tokyo, Japan). The structure of X-ray single-crystal determination was also carried out on a SuperNova Dual (Cu at zero) four-circle diffractometer. Finally, mass spectrum was recorded using the Bruker Daltonics Esquire 6000 mass spectrometer.

2.2. Preparation of H_2L

H_2L was obtained by condensation reactions and the process involving nucleophilic addition and elimination, and the synthetic route was depicted in Scheme 1.



Scheme 1. Synthesis procedure of H_2L .

The synthesis procedure of the non-symmetric salamo-derived ligand (H_2L) could be found in Scheme 1. 2-[O-(1-ethoxyamide)]oxime-2-naphthol and 1,2-bis(aminooxy)ethane were synthesized on the basis of similar approaches [20,50].

Salicylaldehyde (244.1 mg, 2.0 mmol) in ethanol (50 mL) was slowly dropped to 2-[O-(1-ethoxyamide)] oxime-2-naphthol (492.2 mg, 2.0 mmol) in ethanol (30 mL). The solution was stirred at 55 $^{\circ}\text{C}$ for 6 h, cooled to room temperature, and the precipitate was purified with recrystallization from *n*-hexane to obtain the product H_2L . Yield: 551.7 mg, 78.7%. m.p.: 136–138 $^{\circ}\text{C}$. ^1H NMR (500 MHz, $\text{DMSO}-d_6$) δ 10.68 (s, 1H, ArH), 9.97 (s, 1H, ArH), 9.02 (s, 1H, CH=N), 8.65 (d, $J = 8.6$ Hz, 1H, CH), 8.47 (s, 1H, CH=N), 7.88 (d, $J = 8.9$ Hz, 1H, CH), 7.84 (d, $J = 7.8$ Hz, 1H, CH), 7.56 (d, $J = 7.8$ Hz, 1H, CH), 7.54–7.48 (m, 1H, CH), 7.39–7.33 (m, 1H, CH), 7.28–7.23 (m, 1H, CH), 7.21 (d, $J = 8.9$ Hz, 1H, CH), 6.90 (d, $J = 9.1$ Hz, 1H, CH), 6.85 (t, $J = 7.9$ Hz, 1H, CH), 4.54–4.42 (m, 4H, CH_2). (Figure S1) Anal. Calcd for $\text{C}_{20}\text{H}_{18}\text{N}_2\text{O}_4$ (%): C 68.56; H 5.18; N 8.00. Found: C 68.74; H 5.15; N 7.93. UV–Visible (CH_3OH), λ_{max} (nm) (ϵ_{max} , $\text{L}\cdot\text{mol}^{-1}\cdot\text{cm}^{-1}$): 301 (5.61×10^4), 312 (6.80×10^4), 340 (3.11×10^4), 355 (3.13×10^4).

2.3. Preparation of the Cu^{II} Complex

The Cu^{II} complex was obtained by mixing H_2L (3.5 mg, 0.01 mmol) in chloroform (3 mL) with $\text{Cu}(\text{OAc})_2\cdot\text{H}_2\text{O}$ (3.0 mg, 0.015 mmol) in ethanol (5 mL) at room temperature, and the mixed solution color turned to brownish green. The brownish green mixture was filtered, and several single crystals were acquired via natural evaporation method. About one week later, several brownish green block-like single crystals were obtained. Yield: 42.3% (2.90 mg). ESI-FTMS (Figure S2) $m/z = 825.087$ [$\text{Cu}_2\text{L}_2+\text{H}$] $^+$, calc. 824.840; $m/z = 532.982$ [$\text{Cu}(\text{H}_2\text{L})(\text{OAc})_2+\text{H}$] $^+$, calc. 532.920; $m/z = 414.046$ [$\text{Cu}(\text{HL})+\text{H}$] $^+$, calc. 413.920; $m/z = 412.048$. [$\text{Cu}(\text{HL})$] $^+$, calc. 412.920. Anal. Calcd for [$\text{Cu}_3(\text{L})_2(\mu\text{-OAc})_2(\text{H}_2\text{O})_2$] $\cdot 2\text{CHCl}_3\cdot 5\text{H}_2\text{O}$ ($\text{C}_{46}\text{H}_{54}\text{Cl}_6\text{Cu}_3\text{N}_4\text{O}_{19}$) (%): C 40.32; H 3.97; N 4.09; Cu

13.91. Found: C 41.09; H 3.86; N 4.26; Cu 14.25. UV–Visible (CH₃OH), λ_{\max} (nm) (ϵ_{\max} , L·mol⁻¹·cm⁻¹): 314 (7.32×10^4), 369 (3.86×10^4), 401 (2.67×10^4).

2.4. Determination of Single-Crystal Structure of the Cu^{II} Complex

The single-crystal of the Cu^{II} complex with approximate dimensions of $0.22 \times 0.2 \times 0.18$ mm³ was mounted on goniometer head of a SuperNova Dual (Cu at zero) diffractometer. The diffraction data were collected using a graphite mono-chromated Mo-K α radiation ($\lambda = 0.71073$ Å) at 173(2) K. The structure was solved by using the program SHELXS-97 and Fourier difference techniques, and refined by full-matrix least-squares method on F² using SHELXL-2017. The nonhydrogen atoms were refined anisotropically. The hydrogen and carbon atoms of the molecule (C8, H8A and H8B sites occupancy disorder 0.450, and C9', H9'A and H9'B sites occupancy disorder 0.550) are disordered unequally. The crystallographic parameters of the Cu^{II} complex are listed in Table 1.

Table 1. Crystal and refinement parameters data of the Cu^{II} complex.

Compound	The Cu ^{II} Complex
Empirical formula	C ₄₆ H ₅₄ Cl ₆ Cu ₃ N ₄ O ₁₉
Formula weight	1370.25
T, (K)	173(2)
Crystal system	Tetragonal
Space group	I4 ₁ /a
a/(Å)	28.3010(7)
b/(Å)	28.3010(7)
c/(Å)	15.1845(7)
α /(°)	90
β /(°)	90
γ /(°)	90
Volume (Å ³)	12162.0(8)
Z	8
D _{calc} (g/cm ³)	1.497
μ /(mm ⁻¹)	1.373
F(000), e	5592.0
Crystal size/mm ³	0.22 × 0.2 × 0.18
⊖ Range (°)	4.19 to 53.996
Index ranges	-17 ≤ h ≤ 36, -26 ≤ k ≤ 29, -19 ≤ l ≤ 10
Reflections collected	13026
Independent reflections	6539 [$R_{int} = 0.0055$, $R_{\sigma} = 0.0537$]
Data/restraints/parameters	6539/1/395
GOF	1.001
Final R_1 , wR_2 indexes	$R_1 = 0.0441$, $wR_2 = 0.1281$
Final R_1 , wR_2 indexes [all data]	$R_1 = 0.0575$, $wR_2 = 0.1323$
Largest differences peak and hole/ e Å ⁻³	0.41/−1.07

$$R_1 = \frac{\sum ||F_o| - |F_c||}{\sum |F_o|}; wR_2 = \frac{[\sum w(F_o^2 - F_c^2)^2 / \sum w(F_o^2)^2]^{1/2}}{w}; w = [\sigma^2(F_o^2) + (AP)^2 + BP]^{-1}. \text{ Where } P = \frac{(\text{Max}(F_o^2, 0) + 2F_c^2)}{3}; \text{GOF} = S = \frac{[\sum w(F_o^2 - F_c^2)^2 / (n_{\text{obs}} - n_{\text{param}})]^{1/2}}{1}.$$

3. Results and Discussion

3.1. IR Spectra

The main infrared spectra of H₂L and its Cu^{II} complex are given in Table 2. The spectrum of H₂L showed a strong stretching vibration band at about 3216 cm⁻¹ which indicates the presence of multi molecular association and intramolecular hydrogen bonds ($\nu_{\text{O-H}}$). However, this peak disappeared in the Cu^{II} complex, reflecting that the O–H groups of H₂L are wholly deprotonated [51]. A new O–H stretching vibration peak in the Cu^{II} complex was observed at approximately 3420 cm⁻¹ that belongs to the coordination water molecules [52]. The stretching vibration bands at 1609 ($\nu_{\text{C=N}}$) and 1261 cm⁻¹ ($\nu_{\text{Ar-O}}$) of the ligand H₂L were shifted to the low frequencies via ca. 6 and 11 cm⁻¹ upon coordination [53]. Besides, the spectrum of the Cu^{II} complex showed absorption bands at ca. 3425, 1606, and 547 cm⁻¹ which could be assigned to the coordination water molecules, as is substantiated by the results of elemental analyses and the crystal structure [52]. At the same time, the far-infrared spectrum of the Cu^{II} complex was also obtained in the range

of the 100–500 cm^{-1} region so that a distinction could be made between frequencies of the Cu–O and Cu–N bonds, and new peaks of the Cu^{II} complexes were found at ca. 455 and 512 cm^{-1} [54], respectively. These results support the proposal that strong binding participations have occurred in the Cu^{II} complex [39].

Table 2. The main IR bands for H_2L and its Cu^{II} complex cm^{-1} .

Compound	$\nu(\text{O-H})$	$\nu(\text{C=N})$	$\nu(\text{Ar-O})$	$\nu(\text{Cu-O})$	$\nu(\text{Cu-N})$
H_2L	3216	1609	1261	-	-
The Cu^{II} complex	3420	1603	1250	455	512

3.2. UV-Visible Spectra

The UV-Visible spectra of the ligand H_2L and its Cu^{II} complex were tested in methanol solution (1.0×10^{-5} mol/L) at room temperature.

As depicted in Figure 1, the spectrum of H_2L showed four relatively strong absorption peaks at approximately 301, 312, 340, and 355 nm, the absorption peak at 301 nm belongs to the π - π^* transitions of the benzene rings [55]. The peaks at 312, 340, and 355 nm can be attributed to the π - π^* transitions of the C=N bonds of intra-ligand [56]. The absorption peak of the Cu^{II} complex appeared at about 314 nm; this peak could be appointed to π - π^* transitions of the C=N bonds, indicating that coordination reaction occurred between H_2L and the Cu^{II} atoms [56,57]. Simultaneously, two new peaks were found at about 369 and 401 nm, which could be appointed to L \rightarrow M charge-transfer transitions (LMCT). This is characteristic of the metal N_2O_2 -donor complexes [57].

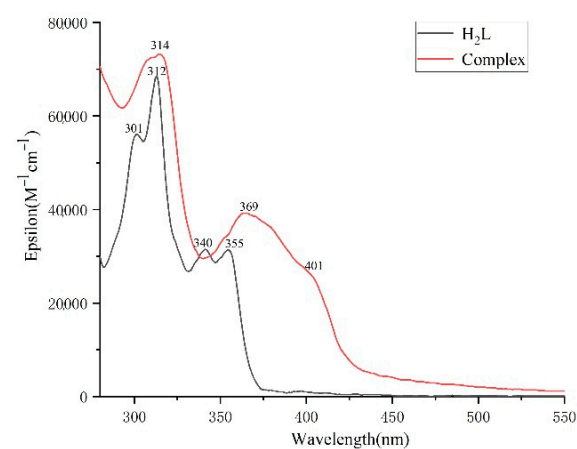


Figure 1. UV-Vis spectra of H_2L and its Cu^{II} complex.

In order to explain the coordination of the ligand H_2L to Cu^{II} ions, the UV-Vis absorption titration experiment was also performed (Figure 2). When the concentration of Cu^{II} ions were added gradually, a new absorption peak appeared between 345 nm and 460 nm, which inferred that the ligand H_2L and Cu^{II} ions coordinate in 1:1.5 ratio to produce a new L- Cu^{II} complex.

3.3. Structure Analysis of the Cu^{II} Complex

The Cu^{II} complex crystallizes in the triclinic system, space group $I4_1/a$. The bond lengths and angles are listed in Table 3. X-ray single-crystal data showed that three Cu^{II} atoms and two completely deprotonated ligand (L^{2-}) moieties produce together a rare homotrimeric 3:2 (M:L) complex with two coordination water molecules and two bi-dentate bridging μ -acetate groups ($\mu\text{-OAc}^-$). This structure differs from the usual mono-nuclear Cu^{II} salamo-based complexes [58]. The six-coordinated terminal Cu^{II} (Cu1) atom is sited at the N_2O_2 cavity containing two phenolic oxygen (O4 and O1) and oxime nitrogen (N2 and N1) atoms in the ligand (L^{2-}) moiety, which forms a basic equatorial plane, and bound to

the other two oxygen (O7 and O5) atoms coming from one coordination water molecule and the $\mu\text{-OAc}^-$ group, respectively, at the end, forming a slightly distorted octahedral geometry. The central Cu^{II} (Cu2) is located on a crystallographic center of inversion. More interestingly, the six-coordinated central Cu^{II} (Cu2) atom is an octahedron, the Cu2 atom is surrounded by O_6 atoms, which involved two completely deprotonated ligand (L^{2-}) moieties and two bridged acetate ($\mu\text{-OAc}^-$) groups (Figure 3a,b). The hydrogen bond data are summarized in Table 4.

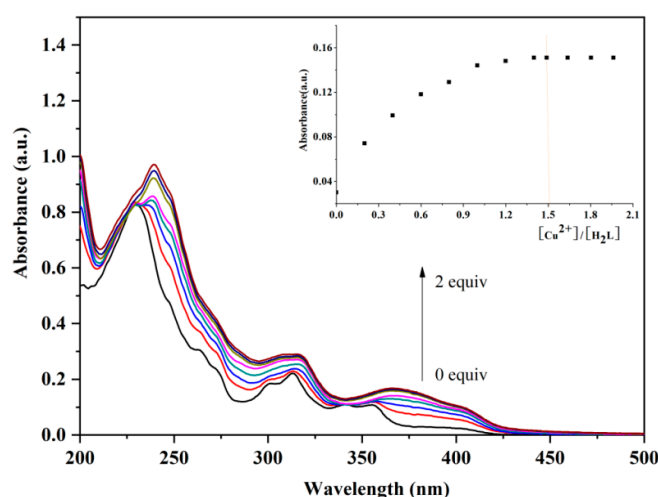


Figure 2. UV-Visible spectrum changes of H_2L (10 μM) upon addition of different amounts of Cu^{II} ions (0~2 equiv.). Inset: The absorbance at 460 nm varied as an interaction of $[\text{Cu}^{2+}]/[\text{H}_2\text{L}]$.

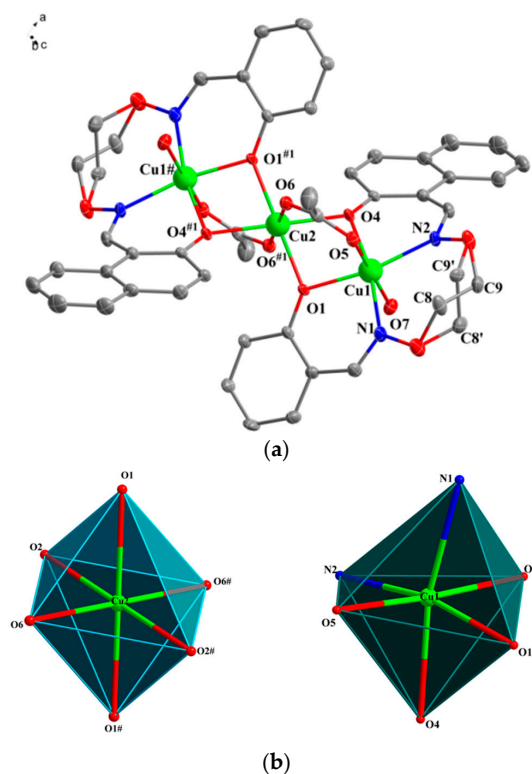
Table 3. Significant bond lengths (\AA) and angles ($^\circ$) of the Cu^{II} complex.

Bond	Lengths	Bond	Lengths
Cu1-O4	2.024(3)	Cu2-O4	2.081(3)
Cu1-O1	2.017(3)	Cu2-O1	2.073(3)
Cu1-O5	2.040(3)	Cu2-O1 [#]	2.073(3)
Cu1-N1	2.072(4)	Cu2-O6	2.063(3)
Cu1-N2	2.063(4)	Cu2-O6 [#]	2.063(3)
Cu1-O7	2.118(3)	Cu2-O4 [#]	2.081(3)
Bond	Angles	Bond	Angles
O1-Cu1-N1	87.90(13)	O1-Cu2-O4 [#]	101.66(11)
O1-Cu1-O4	80.95(11)	O1 [#] -Cu2-O1	180.00(13)
O1-Cu1-O5	90.75(12)	O1 [#] -Cu2-O4	101.66(11)
O1-Cu1-O7	90.15(13)	O1 [#] -Cu2-O4 [#]	78.34(11)
O4-Cu1-O5	92.39(13)	O4-Cu2-O4 [#]	180.00
O4-Cu1-O7	90.94(13)	O6-Cu2-O1	89.50(12)
O4-Cu1-N1	168.25(13)	O6-Cu2-O1 [#]	90.50(12)
O4-Cu1-N2	86.18(13)	O6-Cu2-O4	88.55(12)
O5-Cu1-O7	176.64(13)	O6-Cu2-O4 [#]	91.45(12)
O5-Cu1-N1	91.42(15)	O6-Cu2-O6 [#]	180.00(9)
O5-Cu1-N2	90.92(14)	O6 [#] -Cu2-O4 [#]	88.55(12)
N1-Cu1-O7	85.39(15)	O6 [#] -Cu2-O1	90.50(12)
N2-Cu1-O7	88.92(14)	O6 [#] -Cu2-O1 [#]	89.50(12)
N2-Cu1-N1	104.87(15)	O6 [#] -Cu2-O4	91.45(12)
O1-Cu2-O4	78.34(11)		

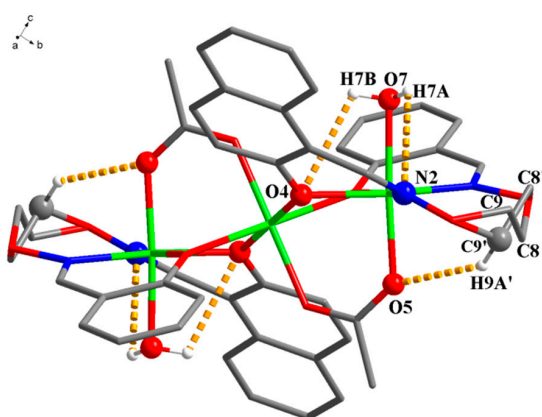
Symmetry transformations used to generate equivalent atoms: ^{#1} 1+x, y, z.

Table 4. Intramolecular hydrogen bonding data [\AA , $^\circ$] of the Cu^{II} complex.

D–H \cdots A	D(D–H)	d(H \cdots A)	d(D \cdots A)	\angle D–H \cdots A	Symmetry Codes
O7–H7A \cdots N2	0.84	2.62	2.930(5)	103	1-x,1-y,-z
O7–H7B \cdots O4	0.82	2.58	2.955(4)	109	1-x,1-y,-z
C9'–H9'A \cdots O5	0.97	2.36	3.181(12)	142	1-x,1-y,-z

**Figure 3.** (a) Crystal structure of the Cu^{II} complex; (b) Coordination polyhedra of the Cu^{II} atoms.

In addition, there are three couple of intra-molecular hydrogen bondings ($\text{C9}'\text{-H9}'\text{A}\cdots\text{O5}$, $\text{O7-H7A}\cdots\text{N2}$ and $\text{O7-H7B}\cdots\text{O4}$) in the Cu^{II} complex [59], as depicted in Figure 4.

**Figure 4.** The intramolecular hydrogen bonds of the Cu^{II} complex.

3.4. Molecular Simulation Calculation of H_2L and Its Cu^{II} Complex

In order to better investigate the structures of H_2L and its Cu^{II} complex, the DMol³ module of MS (Materials Studio) software was used to optimize and simulate the molecules of H_2L and its Cu^{II} complex [60].

The method of structural optimization (property calculation) is GGA, BP (PBE) with the base set DND (DNP), the solvent model (ethanol), the optimization precision set medium, and smooth thermal smearing to speed up the convergence of structural optimization. The molecule energies and frontier molecular orbital energies of H₂L and its Cu^{II} complex are shown in Table 5. For H₂L, it could be found that the calculated energy gap between the LUMO and HOMO of the Cu^{II} complex (0.984 eV) is lower than that of H₂L (1.803 eV) (Figure 5). According to the frontier orbital theory, the photoinduced electron transfer (PET) may be caused by fluorescence quenching [24].

Table 5. Frontier molecular orbital energies and molecule energies of H₂L and its Cu^{II} complex.

Name	Energy/Ha	E _{HOMO} /eV	E _{LUMO} /eV	ΔE/eV
C ₂₀ H ₁₈ N ₂ O ₄ (H ₂ L)	−1183.9	−5.277	−2.917	2.36
C ₄₄ H ₄₂ Cu ₃ N ₄ O ₁₄	−7894.1	−5.014	−3.028	1.986

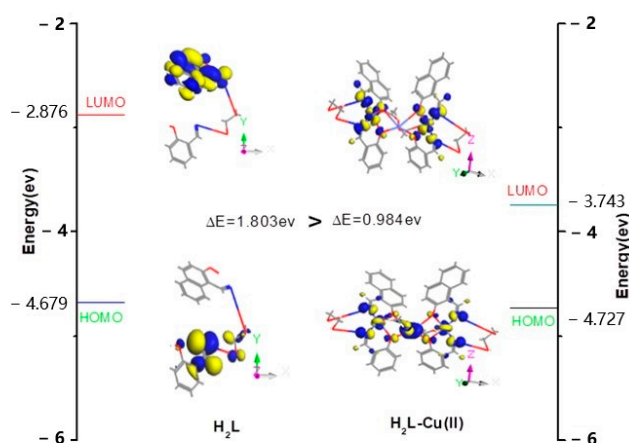


Figure 5. Surface plots of HOMO-LUMO of H₂L (left) and its Cu^{II} complex (right).

3.5. Fluorescence Spectra

The fluorescent properties of the ligand and its Cu^{II} complex were investigated in 1×10^{-5} M ethanol solution at 349 nm excitation wavelength. Corresponding spectra are depicted in Figure 6.

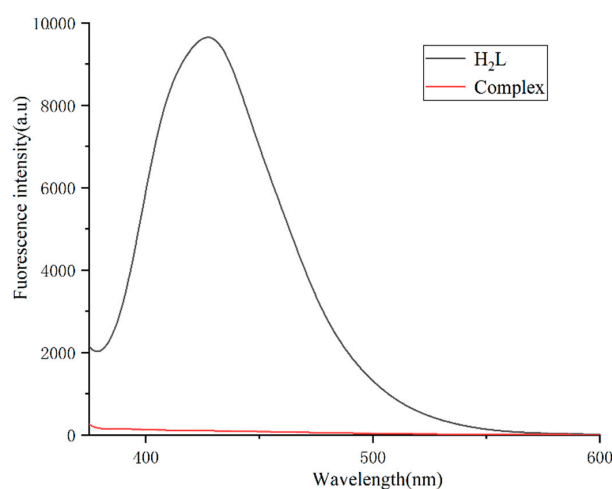


Figure 6. Fluorescent spectra of H₂L and its Cu^{II} complex ($\lambda_{\text{ex}} = 349$ nm).

The Cu^{II} complex underwent fluorescence quenching at 434 nm and the emission peak is red-shifted, this can be appointed to LMCT [61]. Owing to the H₂L molecule's

non-bonding pairs on the oxime N atoms where there is a PET (photoinduced electron transfer) process from the N atom to the benzene ring. Due to the existence of Cu^{II} ions, the fluorescent strength of the system is quenched. This result reflects that Cu^{II} ions interact with the system effectually and have the PET (photoinduced electron transfer) effect, which attenuates the fluorescent strength [62].

3.6. Hirshfeld Surface Analysis

Hirshfeld surface supplies a 3-D figure of inter-molecular inter-actions in the Cu^{II} complex (Figure 7) [63], which could clearly indicate that the surfaces have been mapped over d_{norm} and the corresponding location in shape index exists in the complementary region of red concave surface surrounded by receptors and the blue convex surface surrounding receptors, further proving that such hydrogen bonding exists. The large and deep red spots on the three-dimensional (3D) Hirshfeld surfaces indicate close-contact interactions, which are mainly responsible for the corresponding hydrogen bond contacts. As for the large amount of white region in the d_{norm} surfaces, it is suggested that there is a weaker and farther contact between molecules, rather than hydrogen bonding. The red zone expresses the O–H between the H and O atoms in the Cu^{II} complex. In the interaction intensity figure, the heavier the red area color is, the stronger O–H inter-actions are. As illustrated, the shallower areas mostly represent the spread of influences such as H–H and C–H. As illustrated in the figure, the spread of the approximated hydrogen bonds among the Cu^{II} complex could also be analyzed. This is conducive of investigating inherent elements of the steady existence among the Cu^{II} complex [64].

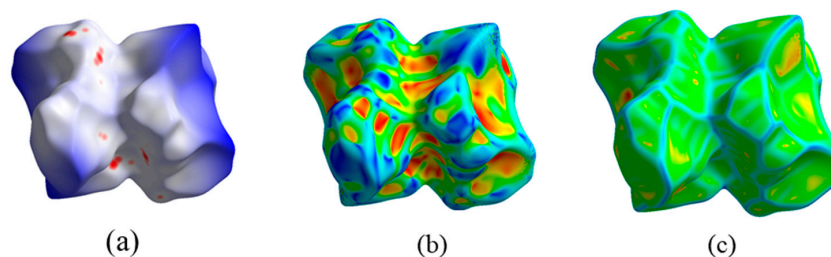


Figure 7. Hirshfeld surfaces analyses mapped with (a) d_{norm} , (b) shape index, and (c) curvedness of the Cu^{II} complex.

In addition, the proportion of C–H/H–C, O–H/H–O, and H–H in the Cu^{II} complex can also be acquired by Hirshfeld surfaces analyses [65–69]. Here, we theoretically calculated the percentages of connects devoted to the total Hirshfeld surface region of the Cu^{II} complex.

As shown in Figure 8, in this 2-D Hirshfeld surface figure, the blue area expresses the distribution of various interactions for the whole Cu^{II} complex. The associated ratios of O–H/H–O, C–H/H–C and H–H/H–H in the surface of Hirshfeld were computed as 8.4%, 18.2%, and 70.2%, respectively.

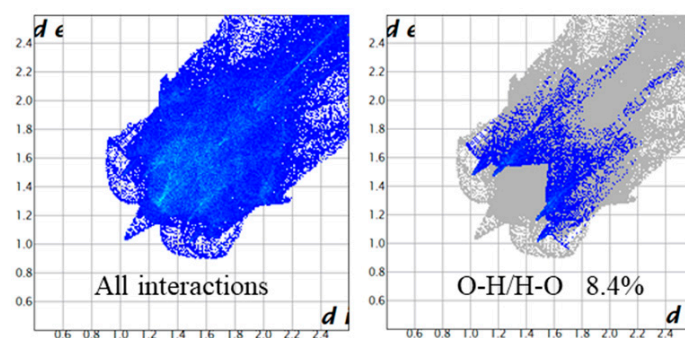


Figure 8. Cont.

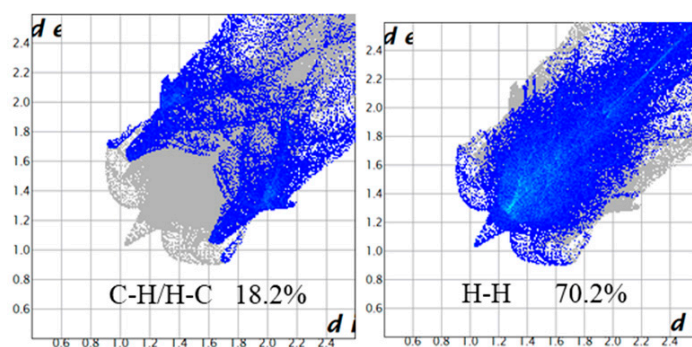


Figure 8. Fingerprint plot of the Cu^{II} complex: full and resolved into $\text{O}\cdots\text{H}$, $\text{C}\cdots\text{H}$ and $\text{H}\cdots\text{H}$ connects reflecting the associated percentages of connects devoted to the whole Hirshfeld surface region of the Cu^{II} complex.

4. Conclusions

In summary, we prepared the non-symmetric salamo-derived ligand H_2L and several single crystals of its Cu^{II} complex. $[\text{Cu}_3(\text{L})_2(\mu\text{-OAc})_2(\text{H}_2\text{O})_2]\cdot 2\text{CHCl}_3\cdot 5\text{H}_2\text{O}$ were cultured by slow evaporation method and various test methods were characterized. Interestingly, the single crystal structure analysis showed that H_2L and Cu^{II} ions form a symmetric trinuclear Cu^{II} complex. The UV-Visible titration clearly showed that the ratio of H_2L to Cu^{II} ions has a 2:3 stoichiometry. Hirshfeld surface analysis indicated that the Cu^{II} complex could be stable due to intra-molecular hydrogen bond interactions.

Supplementary Materials: The following are available online at <https://www.mdpi.com/2073-4352/11/2/113/s1>, Figure S1: ^1H NMR spectrum of H_2L . Figure S2: Mass spectrum of the Cu^{II} complex.

Author Contributions: Y.-D.P. and R.-Y.L. performed the experiments; Y.-X.S. conceived and designed the experiments, and contributed reagents/materials/analysis tools; P.L. analyzed the data. Y.-D.P. and R.-Y.L. wrote the paper. All authors have read and agreed to the published version of the manuscript.

Funding: “This research was funded by National Natural Science Foundation of China, grant number 21761018” and “The APC was funded by Lanzhou Jiaotong University”. The standard spelling of funding agency names at <https://search.crossref.org/funding>.

Institutional Review Board Statement: Not applicable.

Informed Consent Statement: Not applicable.

Data Availability Statement: Not applicable.

Acknowledgments: This work was supported by the National Natural Science Foundation of China (21761018) and the Program for Excellent Team of Scientific Research in Lanzhou Jiaotong University (201706), two of which are gratefully acknowledged.

Conflicts of Interest: The authors declare no competing financial interest.

References

1. Wu, H.L.; Pan, G.L.; Bai, Y.C.; Wang, H.; Kong, J.; Shi, F.; Zhang, Y.H.; Wang, X.L. Preparation, structure, DNA-binding properties, and antioxidant activities of a homodinuclear erbium(III) complex with a pentadentate Schiff base ligand. *J. Chem. Res.* **2014**, *38*, 211–217. [[CrossRef](#)]
2. Song, X.Q.; Liu, P.P.; Liu, Y.A.; Zhou, J.J.; Wang, X.L. Two dodecanuclear heterometallic $[\text{Zn}_6\text{Ln}_6]$ clusters constructed by a multidentate salicylamide salen-like ligand: Synthesis, structure, luminescence and magnetic properties. *Dalton Trans.* **2016**, *45*, 8154–8163. [[CrossRef](#)] [[PubMed](#)]
3. Liu, P.P.; Wang, C.Y.; Zhang, M.; Song, X.Q. Pentanuclear sandwich-type $\text{Zn}^{\text{II}}\text{-Ln}^{\text{III}}$ clusters based on a new salen-like salicylamide ligand: Structure, near-infrared emission and magnetic properties. *Polyhedron* **2017**, *129*, 133–140. [[CrossRef](#)]
4. Wu, H.L.; Wang, C.P.; Wang, F.; Peng, H.P.; Zhang, H.; Bai, Y.C. A new manganese(III) complex from bis(5-methylsalicylaldehyde)-3-oxapentane-1,5-diamine: Synthesis, characterization, antioxidant activity and luminescence. *J. Chin. Chem. Soc.* **2015**, *62*, 1028–1034. [[CrossRef](#)]

5. Zhou, J.J.; Song, X.Q.; Liu, Y.A.; Wang, X.L. Substituent-tuned structure and luminescence sensitizing towards Al³⁺ based on phenoxy bridged dinuclear Eu^{III} complexes. *RSC Adv.* **2017**, *7*, 25549–25559. [[CrossRef](#)]
6. Sun, Y.X.; Pan, Y.Q.; Xu, X.; Zhang, Y. Unprecedented dinuclear Cu^{II} N,O-donor complex: Synthesis, structural characterization, fluorescence property, and Hirshfeld analysis. *Crystals* **2019**, *9*, 607. [[CrossRef](#)]
7. Cui, Y.F.; Liu, C.; Zhang, Y.; Zhang, Y. Newly designed and synthesized heterobimetallic [Cu^{II}–Dy^{III}] salamo-like complex: Structural characterization, DFT calculation, and fluorescent property. *Inorg. Nano-Met. Chem.* **2021**, *51*, 288–295. [[CrossRef](#)]
8. Peng, Y.D.; Zhang, Y.; Jiang, Y.L.; Ren, Z.L.; Wang, F.; Wang, L. An unsymmetric salamo-like chemosensor for fluorescent recognition of Zn²⁺. *J. Fluores.* **2020**, *30*, 1049–1061. [[CrossRef](#)]
9. Mu, H.R.; An, X.X.; Liu, C.; Zhang, Y.; Dong, W.K. Structurally characterized self-assembled heterobimetallic Ni(II)-Eu(III)-salamo-bipyridine coordination polymer: Synthesis, photophysical and antimicrobial properties. *J. Struct. Chem.* **2020**, *61*, 1155–1166. [[CrossRef](#)]
10. Cui, Y.F.; Zhang, Y.; Xie, K.F.; Dong, W.K. A newly synthesized heterobimetallic Ni^{II}-Gd^{III} salamo-bdc-based coordination polymer: Structural characterization, DFT calculation, fluorescent and antibacterial properties. *Crystals* **2019**, *9*, 596. [[CrossRef](#)]
11. Zhang, Y.; Yu, M.; Pan, Y.Q.; Zhang, Y.; Xu, L.; Dong, X.Y. Three rare heteromultinuclear 3d-4f salamo-like complexes constructed from auxiliary ligand 4,4'-bipy: Syntheses, structural characterizations, fluorescence and antimicrobial properties. *Appl. Organomet. Chem.* **2020**, *34*, e5442. [[CrossRef](#)]
12. Zhang, L.W.; Zhang, Y.; Cui, Y.F.; Yu, M.; Dong, W.K. Heterobimetallic [Ni^{II} Ln^{III}] (Ln = Sm and Tb) N₂O₄-donor coordination polymers: Syntheses, crystal structures and fluorescence properties. *Inorg. Chim. Acta* **2020**, *506*, 119534. [[CrossRef](#)]
13. Akine, S.; Sairenji, S.; Taniguchi, T.; Nabeshima, T. Stepwise helicity inversions by multisequential metal exchange. *J. Am. Chem. Soc.* **2013**, *135*, 12948–12951. [[CrossRef](#)] [[PubMed](#)]
14. Chang, J.; Zhang, S.Z.; Wu, Y.; Zhang, H.J.; Sun, Y.X. Three supramolecular trinuclear nickel(II) complexes based on Salamo-type chelating ligand: Syntheses, crystal structures, solvent effect, Hirshfeld surface analysis and DFT calculation. *Transit. Met. Chem.* **2020**, *45*, 279–293. [[CrossRef](#)]
15. Novozhilova, M.V.; Smirnova, E.A.; Polozhentseva, J.A.; Danilova, J.A.; Chepurayeva, I.A.; Karushev, M.P.; Malev, V.V.; Timonov, A.M. Multielectron redox processes in polymeric cobalt complexes with N₂O₂ Schiff base ligands. *Electrochim. Acta* **2018**, *282*, 105–115. [[CrossRef](#)]
16. Bian, R.N.; Wang, J.F.; Li, Y.J.; Zhang, Y.; Dong, W.K. Fluorescent chemical sensor based on double N₂O₂ cavities for continuous recognition of Cu²⁺ and Al³⁺. *J. Photochem. Photobiol. A* **2020**, *400*, 112829. [[CrossRef](#)]
17. Kang, Q.P.; Li, X.Y.; Wang, L.; Zhang, Y.; Dong, W.K. Containing-PMBP N₂O₂-donors transition metal(II) complexes: Synthesis, crystal structure, Hirshfeld surface analyses and fluorescence properties. *Appl. Organomet. Chem.* **2019**, *33*, e5013. [[CrossRef](#)]
18. Wang, J.F.; Li, P.; Li, L.L.; Dong, W.K. A perspective on molecular structure and experimental-computational characterization of a novel Cd(II) pyridine-terminal salamo-like coordination polymer. *Russ. J. Gen. Chem.* **2020**, *10*, 1997–2003. [[CrossRef](#)]
19. Wei, Z.L.; Wang, L.; Guo, S.Z.; Zhang, Y.; Dong, W.K. A high-efficiency salamo-based copper(II) complex double-channel fluorescent probe. *RSC Adv.* **2019**, *9*, 41298. [[CrossRef](#)]
20. Pan, Y.Q.; Xu, X.; Zhang, Y.; Zhang, Y.; Dong, W.K. A highly sensitive and selective bis(salamo)-type fluorescent chemosensor for identification of Cu²⁺ and the continuous recognition of S²⁻, Arginine and Lysine. *Spectrochim. Acta A* **2020**, *229*, 117927. [[CrossRef](#)]
21. Akine, S.; Morita, Y.; Utsuno, F.; Nabeshima, T. Multiple folding structures mediated by metal coordination of acyclic multidentate ligand. *Inorg. Chem.* **2009**, *48*, 10670–10678. [[CrossRef](#)] [[PubMed](#)]
22. Liu, C.; An, X.X.; Cui, Y.F.; Xie, K.F.; Dong, W.K. Novel structurally characterized hetero-bimetallic [Zn(II)₂M(II)] (M = Ca and Sr) bis(salamo)-type complexes: DFT calculation, Hirshfeld analyses, antimicrobial and fluorescent properties. *Appl. Organomet. Chem.* **2020**, *34*, e5272. [[CrossRef](#)]
23. Akine, S.; Dong, W.K.; Nabeshima, T. Octanuclear zinc(II) and cobalt(II) clusters produced by cooperative tetrameric assembling of oxime chelate ligands. *Inorg. Chem.* **2006**, *45*, 4677–4684. [[CrossRef](#)] [[PubMed](#)]
24. Liu, L.Z.; Wang, L.; Yu, M.; Zhao, Q.; Zhang, Y.; Sun, Y.X.; Dong, W.K. A highly sensitive and selective fluorescent “off-on-off” relay chemosensor based on a new bis(salamo)-type tetraoxime for detecting Zn²⁺ and CN⁻. *Spectrochim. Acta A* **2019**, *222*, 117209. [[CrossRef](#)] [[PubMed](#)]
25. Colinas, I.R.; Rojas-Andrade, M.D.; Chakraborty, I.; Oliver, S.R.J. Two structurally diverse Zn-based coordination polymers with excellent antibacterial activity. *CrystEngComm* **2018**, *20*, 3353–3362. [[CrossRef](#)]
26. Lu, X.Y.; Ye, J.W.; Zhang, D.K.; Xie, R.X.; Bogale, R.F.; Sun, Y.; Zhao, L.M.; Zhao, Q.; Ning, G.L. Silver carboxylate metal-organic frameworks with highly antibacterial activity and biocompatibility. *J. Inorg. Biochem.* **2013**, *138*, 114–121. [[CrossRef](#)]
27. Li, X.Y.; Kang, Q.P.; Liu, C.; Zhang, Y.; Dong, W.K. Structurally characterized homo-trinuclear Zn^{II} and hetero-pentanuclear [Zn^{II}₄Ln^{III}] complexes constructed from an octadentate bis(salamo)-based ligand: Hirshfeld surfaces, fluorescence and catalytic properties. *New J. Chem.* **2019**, *43*, 4605–4619. [[CrossRef](#)]
28. Haak, R.M.; Decortes, A.; Escudero, E.C.; Belmonte, M.M.; Martin, E.; Buchholz, J.B.; Kleij, A.W. Shape-persistent octanuclear zinc salen clusters: Synthesis, characterization, and catalysis. *Inorg. Chem.* **2011**, *50*, 7934–7936. [[CrossRef](#)]
29. Yu, M.; Zhang, Y.; Pan, Y.Q.; Wang, L. Two novel copper(II) salamo-based complexes: Syntheses, x-ray crystal structures, spectroscopic properties and Hirshfeld surfaces analyses. *Inorg. Chim. Acta* **2020**, *509*, 119701. [[CrossRef](#)]

30. An, X.X.; Chen, Z.Z.; Mu, H.R.; Zhao, L. Investigating into crystal structures and supramolecular architectures of four newly synthesized hetero-octanuclear $[\text{Cu}^{\text{II}}_4\text{-Ln}^{\text{III}}_4]$ (Ln = Sm, Eu, Tb and Dy) complexes produced by a hexadentate bisoxime chelate ligand. *Inorg. Chim. Acta* **2020**, *511*, 119823. [[CrossRef](#)]
31. Wang, J.F.; Bian, R.N.; Feng, T.; Xie, K.F.; Wang, L.; Ding, Y.J. A highly sensitive dual-channel chemical sensor for selective identification of $\text{B}_4\text{O}_7^{2-}$. *Microchem. J.* **2021**, *160*, 105676. [[CrossRef](#)]
32. Zhang, Y.; Li, Y.J.; Guo, S.Z.; Fu, T.; Zhao, L. A series of heterobimetallic Ni(II)–Ln(III) (Ln = La, Ce, Pr and Nd) coordination polymers derived from 3-EtOsalamo and dicarboxylates: Syntheses, crystal structures and fluorescence properties. *Transit. Met. Chem.* **2020**, *45*, 485–492. [[CrossRef](#)]
33. Zhang, S.Z.; Chang, J.; Zhang, H.J.; Sun, Y.X.; Wu, Y.; Wang, Y.B. Synthesis, crystal structure and spectral properties of binuclear Ni(II) and cubane-like $\text{Cu}_4(\mu_3\text{-O})_4$ cored tetranuclear Cu(II) complexes based on coumarin Schiff base. *Chin. J. Inorg. Chem.* **2020**, *36*, 503–514.
34. Kang, Q.P.; Li, X.Y.; Wei, Z.L.; Zhang, Y.; Dong, W.K. Symmetric containing- PMBP N_2O_2 -donors nickel(II) complexes: Syntheses, structures, Hirshfeld analyses and fluorescent properties. *Polyhedron* **2019**, *165*, 38–50. [[CrossRef](#)]
35. Liu, L.Z.; Yu, M.; Li, X.Y.; Kang, Q.P.; Dong, W.K. Syntheses, structures, Hirshfeld analyses and fluorescent properties of two Ni(II) and Zn(II) complexes constructed from a bis(salamo)-like ligand. *Chin. J. Inorg. Chem.* **2019**, *35*, 1283–1294.
36. Wang, L.; Wei, Z.L.; Chen, Z.Z.; Liu, C.; Dong, W.K.; Ding, Y.J. A chemical probe capable for fluorescent and colorimetric detection to Cu^{2+} and CN^- based on coordination and nucleophilic addition mechanism. *Microchem. J.* **2020**, *155*, 104801. [[CrossRef](#)]
37. Wei, Z.L.; Wang, L.; Wang, J.F.; Guo, W.T.; Zhang, Y.; Dong, W.K. Two highly sensitive and efficient salamo-like copper(II) complex probes for recognition of CN^- . *Spectrochim. Acta A* **2020**, *228*, 117775. [[CrossRef](#)]
38. Wang, L.; Wei, Z.L.; Liu, C.; Dong, W.K.; Ru, J.X. Synthesis and characterization for a highly selective bis(salamo)-based chemical sensor and imaging in living cell. *Spectrochim. Acta A* **2020**, *239*, 118496. [[CrossRef](#)]
39. Pan, Y.Q.; Zhang, Y.; Yu, M.; Zhang, Y.; Wang, L. Newly synthesized homomultinuclear Co(II) and Cu(II) bis(salamo)-like complexes: Structural characterizations, Hirshfeld analyses, fluorescence and antibacterial properties. *Appl. Organomet. Chem.* **2020**, *34*, e5441. [[CrossRef](#)]
40. Liu, C.; Wei, Z.L.; Mu, H.R.; Dong, W.K.; Ding, Y.J. A novel unsymmetric bis (salamo)-based chemosensor for detecting Cu^{2+} and continuous recognition of amino acids. *J. Photochem. Photobio. A* **2020**, *397*, 112569. [[CrossRef](#)]
41. Mu, H.R.; Yu, M.; Wang, L.; Zhang, Y.; Ding, Y.J. Catching S^{2-} and Cu^{2+} by a highly sensitive and efficient salamo-like fluorescence-ultraviolet dual channel chemosensor. *Phosphorus Sulfur Silicon Relat. Elem.* **2020**, *195*, 730–739.
42. Xu, X.; Bian, R.N.; Guo, S.Z.; Dong, W.K.; Ding, Y.J. A new asymmetric salamo-based chemical sensor for dual channel detection of Cu^{2+} and $\text{B}_4\text{O}_7^{2-}$. *Inorg. Chim. Acta* **2020**, *513*, 119945. [[CrossRef](#)]
43. An, X.X.; Zhao, Q.; Mu, H.R.; Dong, W.K. A new half-salamo-based homo-trinuclear nickel(II) complex: Crystal structure, Hirshfeld surface analysis, and fluorescence properties. *Crystals* **2019**, *9*, 101. [[CrossRef](#)]
44. Zhang, Y.; Pan, Y.Q.; Yu, M.; Xu, X.; Dong, W.K. Single-armed salamo-like dioxime and its multinuclear Cu(II), Zn(II) and Cd(II) complexes: Syntheses, structural characterizations, Hirshfeld analyses and fluorescence properties. *Appl. Organomet. Chem.* **2019**, *33*, e5240. [[CrossRef](#)]
45. An, X.X.; Liu, C.; Chen, Z.Z.; Xie, K.F.; Dong, W.K. An unexpected trinuclear cobalt(II) complex based on a half-salamo-like ligand: Synthesis, crystal structure, Hirshfeld surface analysis, antimicrobial and fluorescent properties. *Crystals* **2019**, *9*, 602. [[CrossRef](#)]
46. Li, J.; Zhang, H.J.; Chang, J.; Sun, Y.X.; Huang, Y.Q. Solvent-induced unsymmetric Salamo-like trinuclear Ni^{II} complexes: Syntheses, crystal structures, fluorescent and magnetic properties. *Crystals* **2018**, *8*, 176. [[CrossRef](#)]
47. Yu, M.; Mu, H.R.; Liu, L.Z.; Li, N.; Bai, Y.; Dong, X.Y. Syntheses, structures and Hirshfeld analyses of trinuclear Ni(II) salamo-type complexes. *Chin. J. Inorg. Chem.* **2019**, *35*, 1109–1120.
48. Celedón, S.; Dorcet, V.; Roisnel, T.; Singh, A.; Ledoux-Rak, I.; Hamon, J.R.; Carrillo, D.; Manzur, C. Main-chain oligomers from Ni^{II}- and Cu^{II}-centered unsymmetrical N_2O_2 Schiff-base complexes: Synthesis and spectral, structural, and second-order nonlinear optical properties. *Eur. J. Inorg. Chem.* **2014**, *29*, 4984–4993. [[CrossRef](#)]
49. Liu, X.; Manzur, C.; Novoa, N.; Celedón, S.; Carrillo, D.; Hamon, J.R. Multidentate unsymmetrically substituted Schiff bases and their metal complexes: Synthesis, functional materials properties, and applications to catalysis. *Coord. Chem. Rev.* **2018**, *357*, 144–172. [[CrossRef](#)]
50. Wang, L.; Pan, Y.Q.; Wang, J.F.; Zhang, Y.; Ding, Y.J. A highly selective and sensitive half-salamo-based fluorescent chemosensor for sequential detection of Pb(II) ion and Cys. *J. Photochem. Photobio. A* **2020**, *400*, 112719. [[CrossRef](#)]
51. Zhao, Q.; An, X.X.; Liu, L.Z.; Dong, W.K. Syntheses, luminescences and Hirshfeld surfaces analyses of structurally characterized homo-trinuclear Zn^{II} and hetero-pentanuclear Zn^{II}-Ln^{III} (Ln = Eu, Nd) bis(salamo)-like complexes. *Inorg. Chim. Acta* **2019**, *490*, 6–15. [[CrossRef](#)]
52. Dong, Y.J.; Dong, X.Y.; Dong, W.K.; Zhang, Y.; Zhang, L.S. Three asymmetric salamo-type copper(II) and cobalt(II) complexes: Syntheses, structures and fluorescent properties. *Polyhedron* **2017**, *123*, 305–315. [[CrossRef](#)]
53. Song, X.Q.; Wang, L.; Zheng, Q.F.; Liu, W.S. Synthesis, crystal structure and luminescence properties of lanthanide complexes with a new semirigid bridging furfurylsalicylamide ligand. *Inorg. Chim. Acta* **2013**, *391*, 171–178. [[CrossRef](#)]
54. Dong, X.Y.; Kang, Q.P.; Li, X.Y.; Ma, J.C.; Dong, W.K. Structurally characterized solvent-induced homotrimeric cobalt(II) N_2O_2^- donor bisoxime-type complexes. *Crystals* **2018**, *8*, 139. [[CrossRef](#)]

55. Wang, L.; Wei, Z.L.; Yu, M.; Pan, Y.Q.; Zhang, Y.; Dong, W.K. Multihalogen-substituted salamo-type Mn(II) complexes: Syntheses, crystal structures, Hirshfeld analyses and fluorescence properties. *Chin. J. Inorg. Chem.* **2019**, *35*, 1791.
56. Li, Y.J.; Bian, R.N.; Li, P.; Xie, K.F.; Dong, W.K. Investigation of supramolecular assemblies, Hirshfeld surfaces and DFT analyses, and fluorescence properties of three newly synthesized multinuclear Co(II), Ni(II) and Zn(II) complexes. *Polyhedron* **2020**, *192*, 114867. [[CrossRef](#)]
57. Xu, L.; Yu, M.; Li, L.H.; Ma, J.C.; Dong, W.K. A heterotetranuclear zinc(II)—cerium(IV) salamo complex possessing deca- and dodeca-coordinated cerium(IV) atoms: Synthesis, structure, and photophysical properties. *J. Struct. Chem.* **2019**, *60*, 1358. [[CrossRef](#)]
58. Akine, S.; Taniguchi, T.; Nabeshima, T. Synthesis and characterization of novel ligands 1,2-bis(salicylideneaminoxy)ethanes. *Chem. Lett.* **2001**, *30*, 682–683. [[CrossRef](#)]
59. Zhang, Y.; Liu, L.Z.; Peng, Y.D.; Li, N.; Dong, W.K. Structurally characterized trinuclear nickel(II) and copper(II) salamo-type complexes: Syntheses, Hirshfeld analyses and fluorescent properties. *Transit. Met. Chem.* **2019**, *44*, 627–639. [[CrossRef](#)]
60. Shaan, A.; Monika, T.; Kumar, J.P.; Vinay, G. Insight into the gas phase dissociation of CF₃CH₂I and its reactions with H and OH by first principles. *J. Mol. Model.* **2018**, *24*, 315.
61. Jone Celestina, J.; Tharmaraj, P.; Jeevika, A.; Sheela, C.D. Fabrication of triazine based colorimetric and electrochemical sensor for the quantification of Co²⁺ ion. *Microchem. J.* **2020**, *155*, 104692. [[CrossRef](#)]
62. Bian, R.N.; Xu, X.; Feng, T.; Dong, W.K. A novel O-phenanthroline-based bis(half-salamo)-like chemical sensor: For rapid and efficient continuous recognition of Cu²⁺, HPO₄²⁻ and H₂PO₄⁻. *Inorg. Chim. Acta* **2020**, *516*, 120098. [[CrossRef](#)]
63. Spackman, M.A.; McKinnon, J.J.; Jayatilaka, D. Electrostatic potentials mapped on Hirshfeld surfaces providedirect insight into intermolecular interactions in crystals. *CrystEngCommun* **2008**, *10*, 377–388.
64. Chen, Z.Z.; Zhang, W.Z.; Zhang, T.; Zhang, Y.; Dong, W.K. An insight into the molecular structures, theoretical calculation and catalytic activities of novel heterotrinuclear [Cu^{II}₂Ce^{III}] and heterohexanuclear [Cu^{II}₄Y^{III}₂] bis(salamo)-based complexes. *New J. Chem.* **2020**, *44*, 19836–19849. [[CrossRef](#)]
65. Xu, X.; Wang, J.F.; Bian, R.N.; Zhao, L. Synthesis, structure, Hirshfeld analysis and fluorescence properties of a new asymmetric salamo-based ligand and its Cu(II) complex involving oxime oxygen coordination. *J. Coord. Chem.* **2020**, *15*, 2209–2223. [[CrossRef](#)]
66. Spackman, M.A.; Jayatilaka, D. Hirshfeld surface analysis. *CrystEngCommun* **2009**, *11*, 19–32. [[CrossRef](#)]
67. Wang, J.F.; Li, R.Y.; Li, P.; Dong, W.K. Exploring coordination behaviors, structural characterizations and theoretical calculations of structurally different Cu(II), Co(II) and Ni(II) emissive complexes constructed from a salamo-based ligand and 4,4'-bipy. *Inorg. Chim. Acta* **2021**, *518*, 120247. [[CrossRef](#)]
68. Xu, X.; Feng, T.; Feng, S.S.; Dong, W.K. Influence of structural variation of salamo-based ligand on supramolecular architectures, Hirshfeld analyses, and fluorescence properties of new tetranuclear Ni(II) complexes. *Appl. Organomet. Chem.* **2021**, *35*, e6057. [[CrossRef](#)]
69. Wang, J.F.; Xu, X.; Bian, R.N.; Dong, W.K.; Ding, Y.J. Investigation on structurally different Cu(II) and Ni(II) complexes constructed from a novel pyridine-terminal salamo-like ligand. *Inorg. Chim. Acta* **2021**, *516*, 120095. [[CrossRef](#)]